Experiments in Fluids (2006) 41: 441–451
DOI 10.1007/s00348-006-0171-4

RESEARCH ARTICLE

Mario Felli · Fabio Di Felice · Giulio Guj
Roberto Camussi

"Analysis of the propeller wake evolution by pressure and velocity phase measurements"

Received: 9 March 2006 / Revised: 25 May 2006 / Accepted: 25 May 2006 / Published online: 11 July 2006

Abstract In the present study an experimental analysis of the velocity and pressure fields behind a marine propeller, in non-cavitating regime is reported. Particle image velocimetry measurements were performed in phase with the propeller angle, to investigate the evolution of the axial and the radial velocity components, from the blade trailing edge up to two diameters downstream. In phase pressure measurements were performed at four radial and eight longitudinal positions downstream the propeller model at different advance ratios. Pressure data, processed by using slotting techniques, allowed reconstructing the evolution of the pressure field in phase with the reference blade position. In addition, the correlation of the velocity and pressure signals was performed. The analysis demonstrated that, within the near wake, the tip vortices passage is the most important contribution in generating the pressure field in the propeller flow. The incoming vortex breakdown process causes a strong deformation of the hub vortex far downstream of the slipstream contraction. This process contributes to the pressure generation at the shaft rate frequency.

1 Introduction

Hydrodynamic-induced noise and vibrations has become a very important problem in the last years both in navy and civil naval architecture, in view of the increasing ship speed required, the high propeller thrust to be supplied and the need of comfortable vessels. Vibratory forces, which are predominantly applied at the blade frequency, have frequently caused local structural failures by fatigue effects and, in many cases, have precluded the occupancy of parts of passenger vessels because of the noise and discomfort correlated to the resonance of decks and bulkheads.

The problem of reducing propeller induced noise and vibration has led to an increased complexity of the blade geometry, primarily due to the need of low aspect ratio and of skewed shapes, and has implied a rising interest on detailed measurements of the propeller flow field, to be used for both new design approaches as well as for analyzing propulsive, hydro-acoustic, and structural performances.

The pressure on the stern bottom of the hull, generated by a propeller, is strictly related to the induced velocity field. Therefore a detailed flow field analysis, relating the flow structures and the pressure signal, is required to improve the knowledge on the noise mechanism. Experimental investigation also provides baselines to improve and integrate theoretical predictions and support the flow modeling and the validation of computational codes (BEM, RANS, LES).

The flow field analysis around a propeller is complicated by many factors as unsteadiness, three-dimensionality, and high turbulence levels. These properties have been pointed out in many previous laser doppler velocimetry (LDV) measurements (Min 1978; Kobayashi 1982; Cenedese et al. 1985; Hoshino et al. 1987), but none of previous studies provided correlations between the velocity field and pressure signals. In the present study the pressure signals were correlated with the flow structures of the propeller slipstream, like the tip and hub vortex and the blade wake. Using 2D-PIV and hydrophones performs the correlation between the velocity field and the pressure at a point.

A Wageningen modified type model propeller (INSEAN E779A) was selected for the present research

M. Felli (✉) · F. Di Felice
INSEAN, Italian Ship Model Basin,
Via di Vallerano 139, 00128 Rome, Italy
E-mail: m.felli@insean.it
Tel.: +39-06-50299240
Fax: +39-06-5070619

G. Guj · R. Camussi
Department of Mechanical and Industrial Engineering,
"Roma Tre" University, Via della Vasca Navale 79,
00146 Rome, Italy

project for two main reasons. First, this model propeller has been widely studied in the past with the most advanced flow measurement and visualization techniques, such as LDV (Cenedese et al. 1985; Stella et al. 2000a) and PIV (Di Felice et al. 2004). A large amount of data has been collected providing a thorough documentation on the non-cavitating flow characteristics: the propeller geometry, LDV data, and PIV data are now freely available for downloading at http://www.crm.insean.it/E779A.

2 Experimental set up and flow conditions

2.1 Facility and propeller model

Measurements were conducted in the Italian Navy Cavitation Tunnel (C.E.I.M.M.) This is a close jet tunnel with a 2.6 m long × 0.6 m span × 0.6 m deep test section. Perspex windows on the four walls enable optical access.

The nozzle contraction ratio is 5.96:1 and the maximum water speed is 12 m/s. The highest free stream turbulence intensity in the test section is 2%, and, in the adopted test condition, reduces to 0.6% in the propeller blade inflow at 0.7 r/R, r being the radial coordinate, and R the propeller radius. In the test section, the mean velocity uniformity is within 1% for the axial component and 3% for the vertical component.

The four blades propeller model E779A was used for the tests. This is a Wageningen modified type model, widely studied with the most advanced flow measurement and visualization techniques (Cenedese et al. 1985; Stella et al. 2000b; Di Felice et al. 2004). Overall details of the propeller are summarized in Table 1.

Two reference systems are adopted:

(a) Cartesian reference frame O-XYZ with the origin O in the intersection between the propeller disk and the rotation axis, the X axis downstream-oriented along the tunnel centerline, the Y axis along the upward vertical, and the Z axis along the horizontal towards starboard.
(b) Cylindrical reference frame O-$XR\theta$ with the origin O in the intersection between the propeller disk and the rotation axis, the X axis downstream-oriented along the propeller axis, the R axis along the radial outward, the θ axis along the azimuth.

Two dimensionless groups govern the propeller flow field in non-cavitating conditions: the advance ratio $J = U_\infty/2nR$, where U_∞ is the free stream velocity, n the revolution frequency and $2R$ the diameter of the propeller, and the Reynolds number $Re = C_{0.7}V_{0.7}/\upsilon$, where $C_{0.7}$ and $V_{0.7}$ are, respectively the chord of the blade and the velocity at 0.7 r/R and υ the kinematic viscosity.

Table 1 E779A model propeller features

Number of blades	4
Diameter (mm)	272
Pitch–diameter ratio	1.1
Boss diameter max (mm)	45.5
Rake (degree)	4° 3″
Developed area–disk area ratio	0.688

2.2 PIV experimental set up

A sketch of the PIV experimental set up is reported in Fig 1. The propeller model is mounted on a front dynamometer shaft. This arrangement of the propeller and the length of the test section, which is about 15 times the propeller diameter, allows the slipstream to develop freely in the downstream direction as in a real operative condition. An encoder, with a resolution of 0.1°, mounted on the dynamometer shaft, feeds a special signal processor, which provides a trigger signal to a synchronizing device for each angular position of the reference blade. The synchronizer provides a TTL trigger signal to a cross-correlation camera (1,008 × 1,018 px), and to a double cavity Nd-Yag laser (200 mJ/pulse at 12.5 Hz each), to allow image acquisitions in phase with the propeller angular position. The digital cross-correlation video camera, allows the recordings of two separate images (one for each laser pulse) within a few microseconds at a maximum camera frame rate of 15.0 Hz. By using cross-correlation, the directional ambiguity is completely removed. The instantaneous velocity fields were acquired from a distance up to 700 mm from the side window, using a 60 mm lens with 2.8 f number and imaging an area of about 100 × 100 mm.

The choice of tracer particles is one of the critical aspects of the PIV technique, especially in case of large facilities. Since the technique is based on the measurement of particle displacement, it is fundamental that the seed accurately follows the water flow velocity. This requires particles having a diameter on the order of few micrometers. At the same time, it is mandatory to achieve a high uniform seeding density in the region of interest, at least 15-particle pairs/interrogation window, in order to accurately perform auto/cross correlation analysis. To this purpose, the water in the tunnel was initially filtered, and then seeded with 10 μm silver coated hollow glass spherical particles with high diffraction index and density of about 1.1 g/cm^3. The PIV system was arranged to measure, in the mid longitudinal plane of the propeller, the axial and vertical velocity components simultaneously. In view of the symmetry of the propeller inflow and of the steady conditions, when the light sheet is located on the X-Z plane, the axial component of the velocity (component along the X axis) and the vertical one (component along the Z axis) correspond, respectively to the axial and the radial components in the propeller moving frame O-$XR\theta$.

To investigate the propeller wake up to two diameters downstream the blades trailing edge, measurements were performed over three adjacent windows by traversing the camera (with an accuracy of about 0.1 mm). The

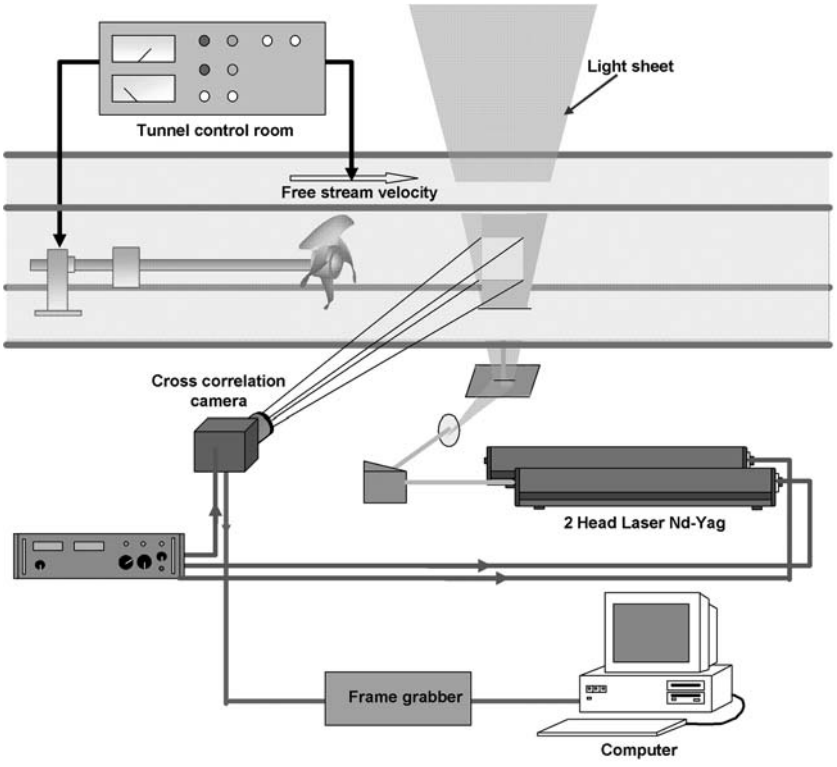

Fig. 1 PIV measurements experimental set up

initial reference position was fixed with an accuracy of about 0.5 mm by imaging a special target device.

The PIV image analysis was carried out using an iterative algorithm, described in Di Florio et al. (2002). A recursive processing method, which implements the window-offset technique (Westerweel 1997) and gaussian weighting, was used to reduce the size of the interrogation area and to increase the spatial resolution. The analysis was realized by using a final window of 24×24 px, with a limited number of spurious determinations (less then 8%) and a spatial resolution equivalent to 2.4×2.4 mm. At a given angular position of the reference blade, 65 couples of images were acquired, to evaluate axial, and radial mean velocity component and turbulence field. The range 0°–85° with a step of 5° was investigated. Further information on the PIV image processing is reported in Di Felice et al. (2004).

2.3 Pressure measurements experimental set up

Pressure measurements were performed by using hydrophones (Bruel and Kjaer 8103 models), because of their high dynamic range from 0.3 to 20 kHz. Four hydrophones were mounted on a rake device, shown in Fig 2. The transducers outputs were amplified by conditioner-amplifiers Bruel and Kjaer 2650 with band pass filter (0.3– 20 kHz), connected with the acquisition system and a spectral analyzer. Simultaneously, the TTL signal was acquired to synchronize the angular position of the reference blade. Specifically, such a synchronization was accomplished during the post processing, using a slotting technique and arranging the pressure data inside 200 angular slots, 1.8° wide,

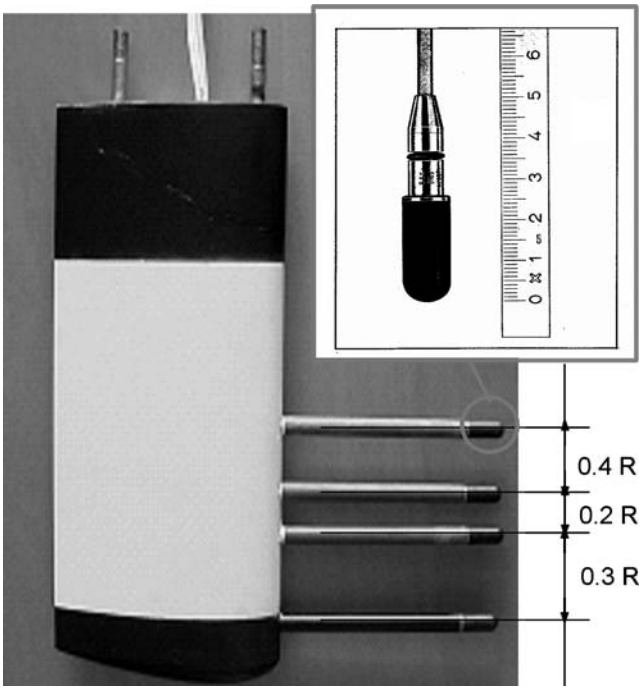

Fig. 2 Hydrophones arrangement

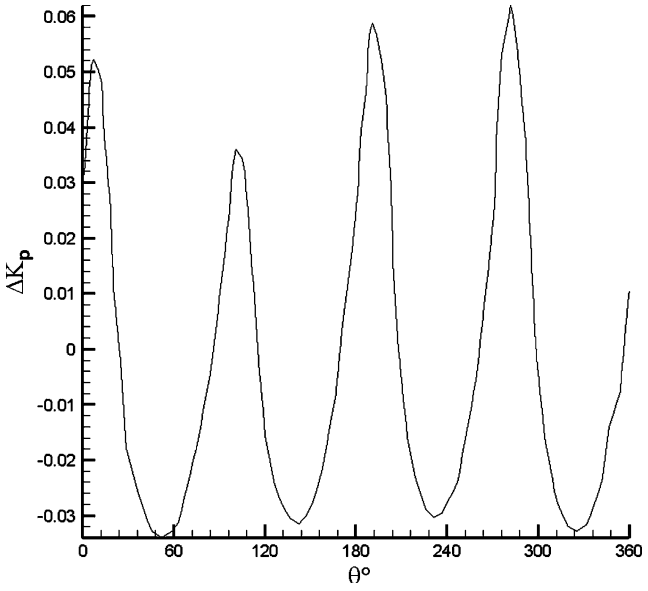

Fig. 3 Phase averaged pressure signals at $x = 0.5R$, $r/R = 0.9$ for $J = 0.88$, $V = 5$ m/s and $n = 25$ rps

depending on the phase delay from the last trigger signal [more details on the so called time triggering technique, are given in Stella et al. (2000a)]. Finally, the phase averaged pressure coefficient Δk_p, is evaluated as:

$$\Delta k_p = \frac{\Delta P}{\rho n^2 D^2} \quad (1)$$

with ΔP denoting the total pressure fluctuations.

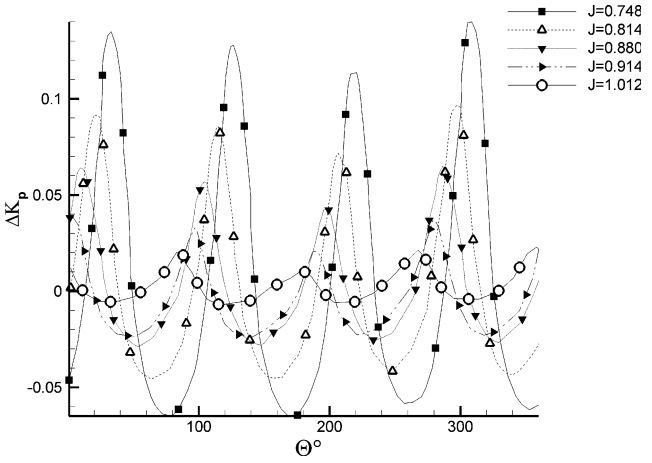

Fig. 4 Same as previous plot but for different J

The hydrophones signals were acquired for 50 s at the sample rate of 40 kHz.

The pressure measurements were performed at four radial and eight longitudinal positions downstream of the propeller model. Pressure signals acquisition was performed at several propeller conditions $J = 0.748$, 0.814, 0.880, 0.940, 1.012 that correspond to Re ($Re \times 10^6$) 1.14, 1.15, 1.17, 1.80, 1.20. Correlation between pressure signal and velocity field was performed only for $J = 0.88$.

Fig. 5 Correlation between velocity field, by PIV images, and pressure signal at $\theta = 20°$. The longitudinal station corresponds to $x/R = 1.0$. Marks in the contour plot gives evidence of the pressure probe positions

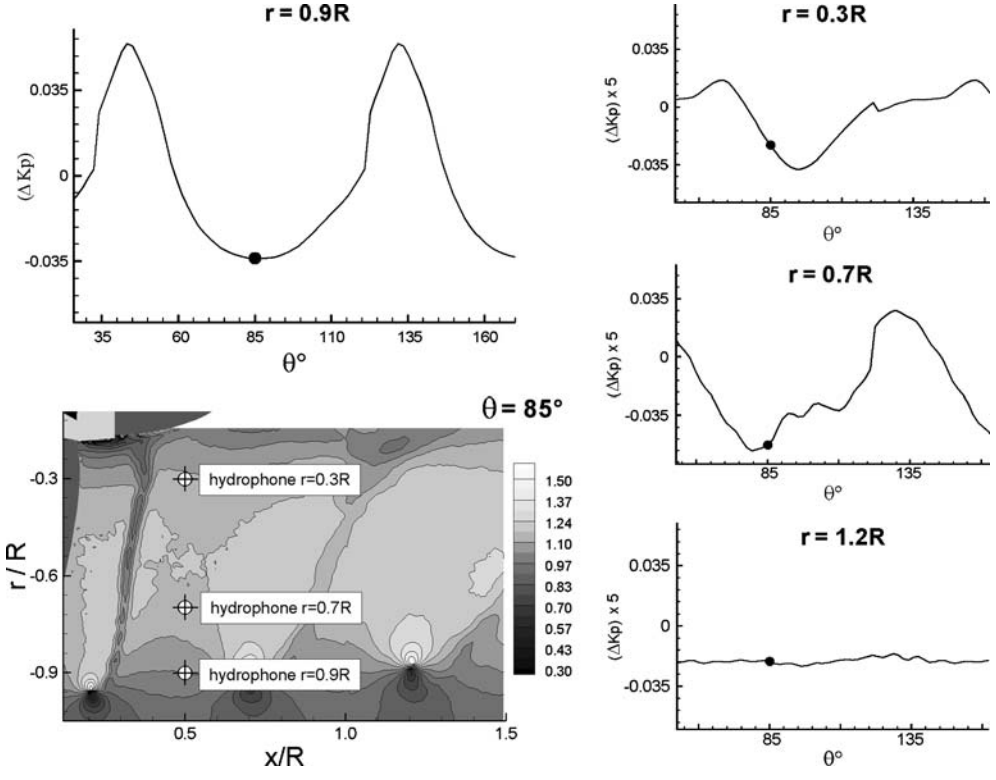

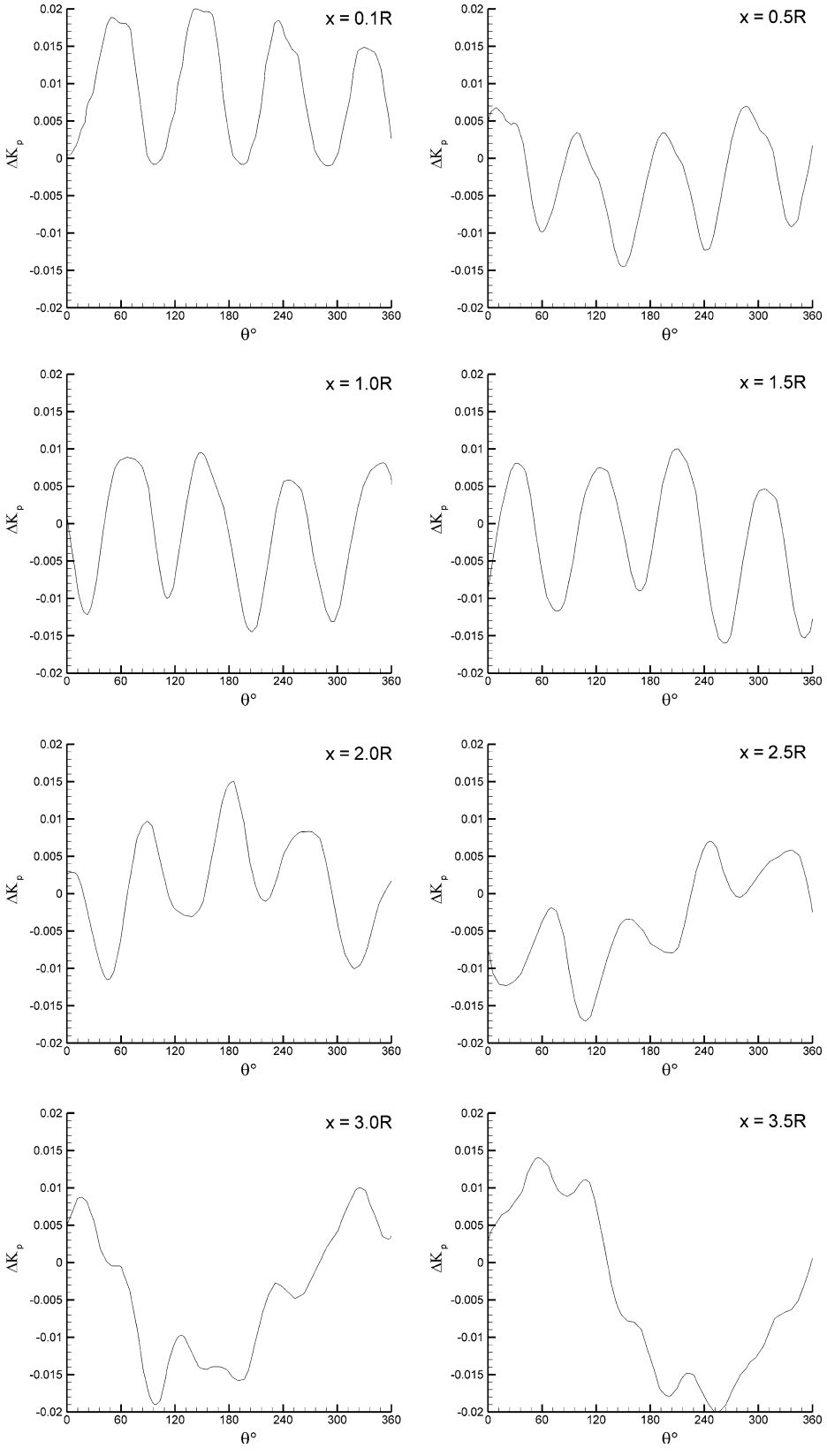

Fig. 6 Longitudinal evolution of the phase averaged pressure signal at $r/R = 0.3$, $J = 0.748$

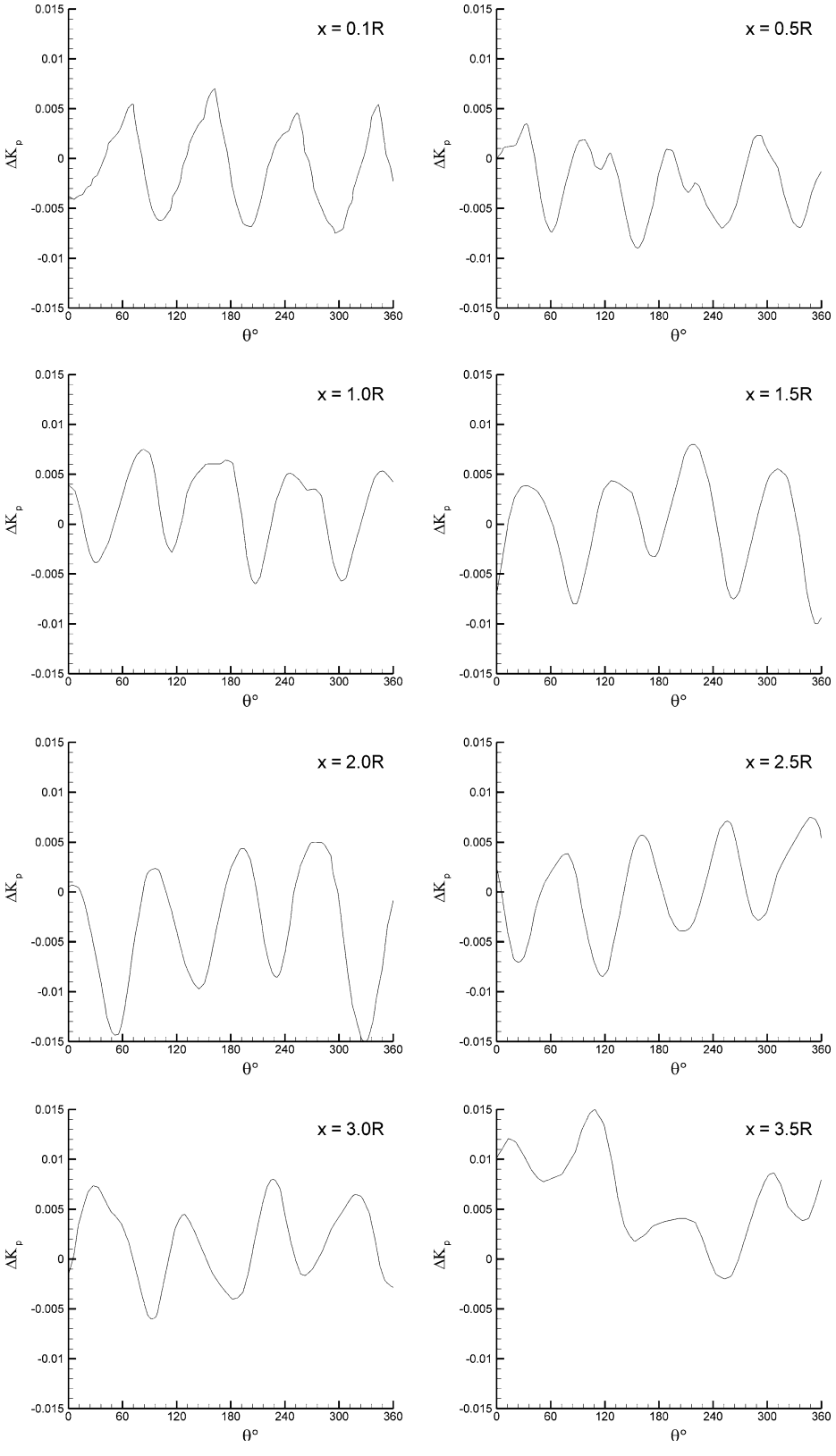

Fig. 7 Longitudinal evolution of the phase averaged pressure signal at $r/R = 0.3$, $J = 0.88$

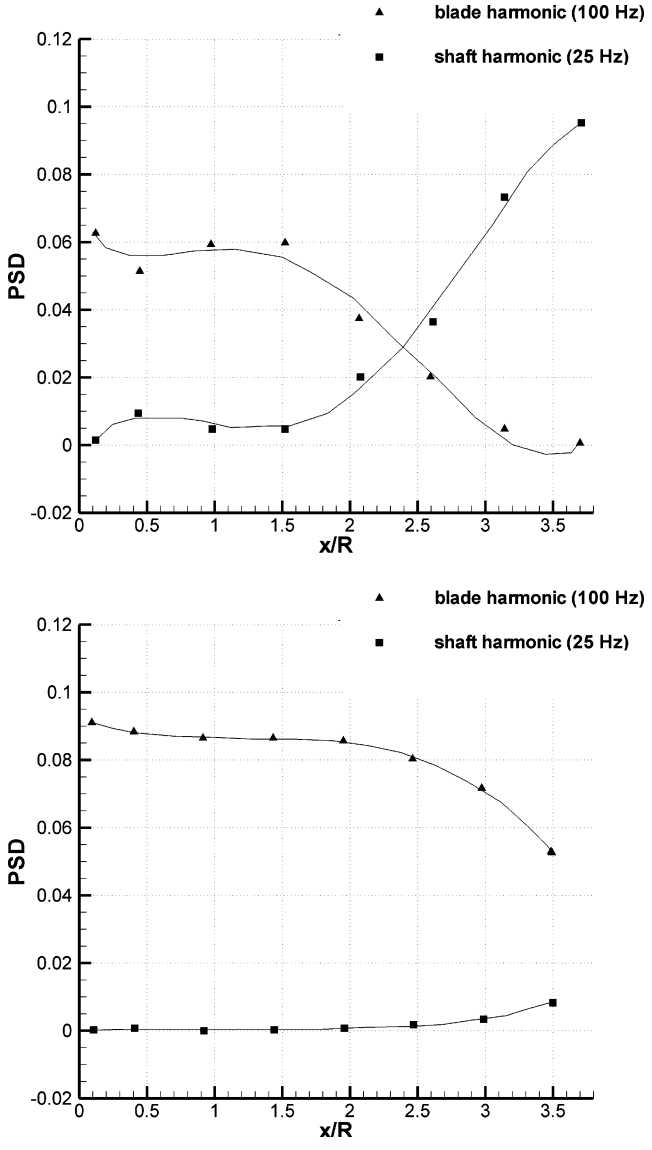

Fig. 8 Amplitude of power spectral density of the pressure signals for the blade rate (*triangles*) and shaft harmonics (*squares*) as a function of x/R, for r = $0.3R$ (*top*), and $r = 0.9R$ (*bottom*) and $J = 0.748$

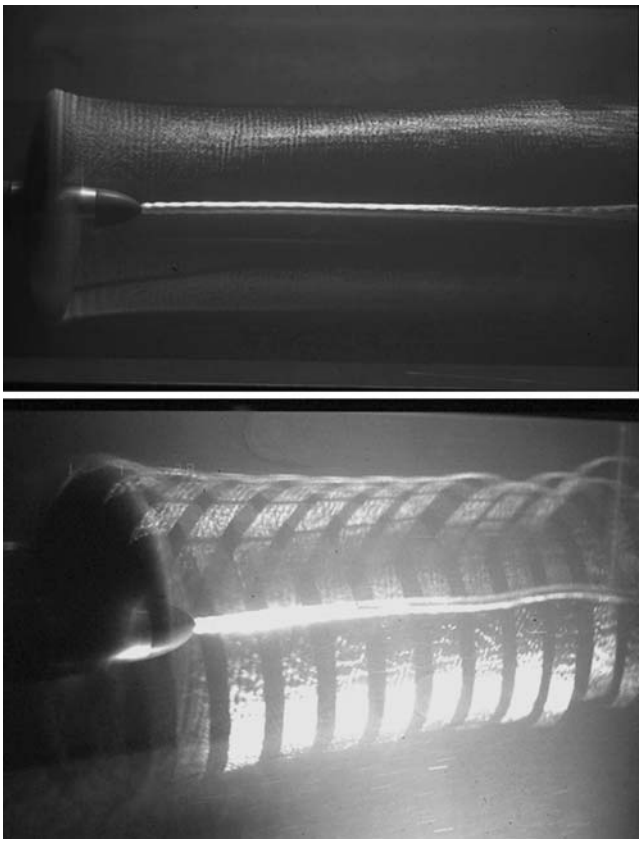

Fig. 9 Visualizations of the streamtube instability in cavitating condition. A lateral view is reported in the upper panel while the lower panel reports an inclined view from behind

3 Experimental results

In the following we will focus on pressure measurement results and the correlation of the pressure signal with the flow structures.

In the case of non-cavitating propeller, the pressure field, at a fixed point in space, shows periodical fluctuations at a fundamental frequency corresponding to the blade-passing rate (25 Hz). An example of Δk_p is shown in Fig. 3 at the position $x/D = 0.5$ and $r/R = 0.9$. Four peaks of the pressure coefficient identify the traces of the tip vortices shed from the four blades, with a phase delay of 90° each. Some differences among the peaks can be noticed as a consequence of small differences in the blades geometries, already pointed out in previous analyses performed on the same propeller model (Cenedese et al. 1985; Stella et al. 2000b; Di Felice et al. 2004) and recently confirmed by an accurate mapping of the blades.

As suggested in Tachmindji (1957), the amplitude of the pressure fluctuations reduces when increasing the advance coefficient because of the reduced loading and intensity of the tip vortex. This is pointed out in Fig. 4 where the signals are shifted to take into account for the different pitch to diameter ratio of the wake with J.

An example of the pressure signals and the flow field measured by PIV for the angular position $\theta = 20°$ is reported in Fig. 5 (where θ denotes the reference blade angular position). The contour plot represents the magnitude of the in-plane velocity components normalized with the free stream velocity. The main flow structures, like the viscous wake shed from the blade trailing edge, the tip and the hub vortex, are clearly apparent. In the same figures the pressure at the hydrophones locations is also highlighted. The pressure coefficients at different radial positions, for the longitudinal station $x/R = 1.0$ are also reported. The signals show a different behavior and amplitude as a consequence of the different interaction with the flow structures of the propeller wake.

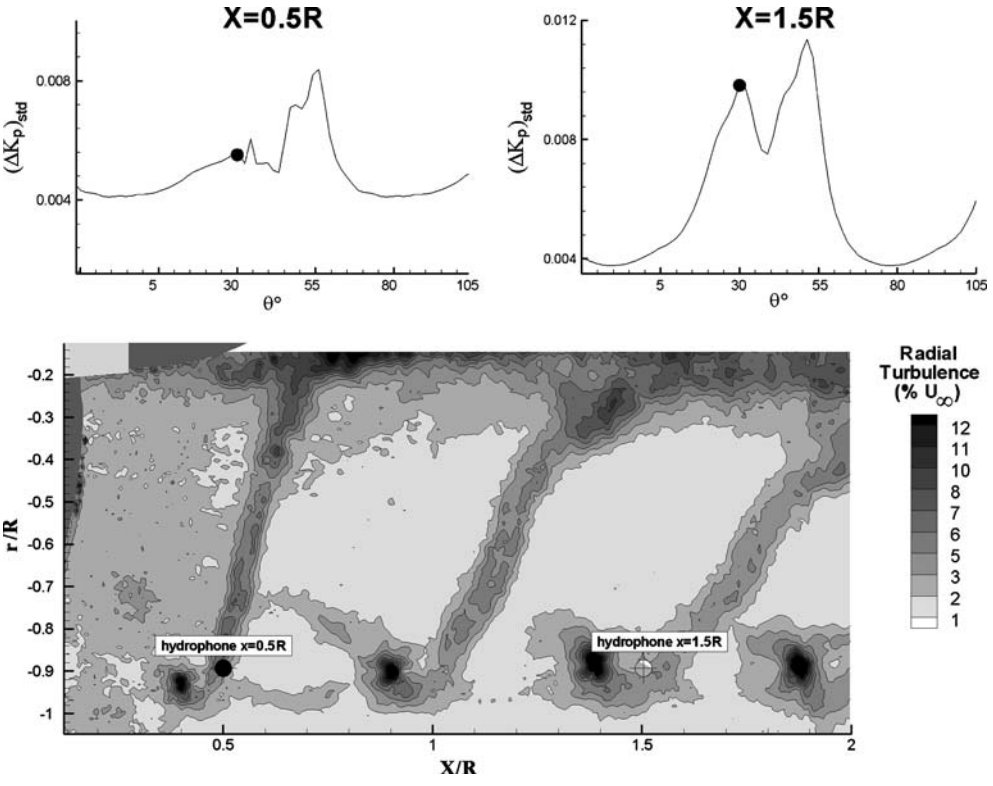

Fig. 10 Correlation between the radial relative turbulence level and pressure signal standard deviation at $\theta = 30°$ and for two different x/R (*red* and *blue* marks reported in the contour plot)

It is shown that the pressure signal at $r/R = 0.3$ is influenced by the blade wake passages and by the hub vortex evolution. In the same way, at $r/R = 0.7$, the signal consists of large scale fluctuations caused by the passage at the hydrophone location of the low pressure flow, coming from the face of the propeller and small scale fluctuations due to the passage of the blade wake.

The maximum values of the pressure coefficient are achieved at $r/R = 0.9$ simultaneously to the passage of the tip vortex core. This result clarifies that the tip vortex is the most important pressure fluctuation source in the propeller wake at $x/R = 1.0$. In fact pressure fluctuation peaks are one order of magnitude larger at $r/R = 0.9$ with respect the other locations. At $r/R = 1.2$ the pressure fluctuation is very low, the transducer being out of the slipstream tube. Close to the trailing edge of the propeller and for all the radial positions the pressure signals are dominated by the blade rate.

Further downstream, in the transition wake, the blade rate frequency is gradually lost and replaced by lower frequency corresponding to the shaft rate as the distance from the propeller disc increases (Fig. 6). This behavior connected with the instability process of the wake, takes place as close to the propeller disk as the propeller load increases, as it is clearly evident from the comparison between the plots of Figs. 6 and 7. Actually the bigger the blade loading condition the faster is the transition to the instability of the propeller wake (Di Felice et al. 2004). Figure 8 shows the amplitude of the blade rate and shaft harmonics, for the radial position $r/R = 0.3$ (top of Fig. 4) and $r/R = 0.9$ (bottom of Fig. 4). The analysis points out that near the hub ($r/R = 0.3$) and 2–3 diameters downstream the propeller, a different mechanism is contributing to the generation of the pressure signal. In fact the transfer of the energy from the blade to the shaft rate harmonics is strictly related to the mechanism of the streamtube instability. Downstream of the contraction a separation of the trajectory of the tip vortices occurs, due to the different blades and a strong spiraling and deformation process of the hub vortex. The slipstream starts to lose its axis-symmetry and blade periodicity but the first phase of the breakdown still maintains the phase with the shaft revolution. More specifically, the streamtube starts to describe a precession motion around the hub vortex as shown by the visualizations of Fig. 9: at the end of the transition wake the envelope of the tip vortices trajectories, describing a cylindrical surface in a reference frame fixed along the hub vortex trajectory, tends to gradually diverge to a conical geometry when seen from a fixed reference frame as a consequence of the strong deformation of the hub vortex. The starting point of such an instability seems to be the interaction between the actual blade wake and the tip vortex of the previous one (Di Felice et al. 2004), that takes place because of the different pitch angle of their helical paths.

The phase analysis of the correlation between the turbulence field with the standard deviation of the pressure signal $(\Delta k_p)_{std}$ was also performed. An example of the achieved results is reported in Fig. 10.

It is observed that the highest values of the pressure standard deviation are related to the highest

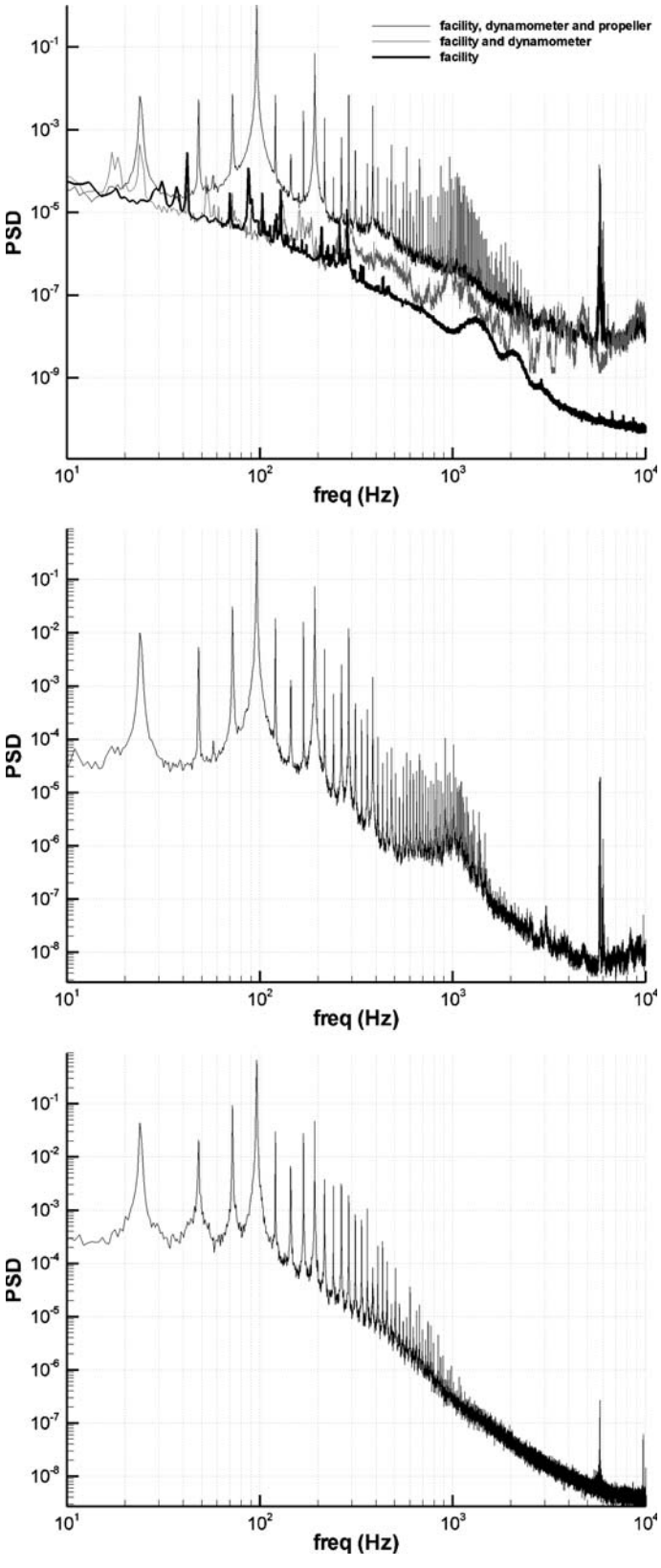

Fig. 11 Power spectral density of the pressure signals. *Top* spectrum of the pressure signal in the propeller wake at $r = 0.9$ and $x = 0$ and background contribution (flow measurements without the propeller installed at the same conditions of the tests) with (*black*) and without (*blue*) the dynamometer in rotation. *Mid* spectrum of the pressure signal in the propeller wake at $r = 0.9$ and $x = 2R$. *Bottom* spectrum of the pressure signal in the propeller wake at $r = 0.9$ and $x = 3$R

values of the turbulence intensity and mainly concentrated, at $r/R = 0.9$, in the tip vortex core. Furthermore, the turbulent blade wake, downstream of the propeller, is quickly diffused and dissipated by viscous effects. Nevertheless the standard deviation plots show two peaks associated, respectively to blade wake and

tip vortex passages. The maximum values are achieved in correspondence of the tip vortex core. Finally, it is shown that the standard deviation of the pressure fluctuation in the downstream direction rises as a consequence of the largest turbulent fluctuation achieved in the tip vortex core far downstream the propeller. This effect is related to the vortex breakdown instability as was shown in Di Felice et al. (2004).

Figure 11 shows the power spectral density of the pressure signals for three different longitudinal positions at $r = 0.9R$. Background noise of the facility, measured at $r = 0.9R$ and $x = 0.1R$ without the propeller installed and with the dynamometer stopped, is also shown in Fig. 11.

The energy content for the pressure signals distributes itself along three different contributions:

(a) The shaft and blade harmonics and their multiples, whose relative intensities change with the distance from the propeller disc due to the instability mechanism of the streamtube, already pointed out in Fig. 4.
(b) A background spectral contribution between 0.7 and 1 kHz that appears also when the dynamometer is switched off and the propeller removed, probably due to the facility impeller engine.
(c) A contribution around 6 kHz due to a high-peaked noise, whose origin seems to have reference to the phenomenon of "singing propeller" (Saunders 1957). This sound is a harmonic tone whose origin is the frequency of the Von Karman vortices shedding from the blade trailing edge, having a finite curvature. The value of the vortex-trail frequency can be estimated as follows:

$$f = \frac{St \cdot U_{\text{blade}}}{d}$$

where, St is the Strouhal number, f the audible frequency, d the effective diameter of the rounded trailing edge and U_{blade} the blade relative conventional velocity. For the present case the magnitude of such a frequency is calculated on the basis of the Strouhal number past a cylinder at high Reynolds number, fixing U_{blade} equal to the relative blade velocity at $0.7R\text{V}_{0.7}$ and measuring by optic techniques the trailing edge curvature. The achieved dimensional frequency matches with the results of Fig. 11. Furthermore, the absence of the above peak in the background spectra (measurements without the propeller installed) acquired at the same test conditions, with and without the dynamometer in rotation, seems to confirm this thesis (Fig. 11, top). The different combinations between the blade curvatures in the trailing edge (ranging between 0.3 and 0.8 mm), and the blade velocity (that depends on the radius) justify the occurrence of different contributions around 6 kHz. The intensity of such a peak decreases with the distance from the propeller disk probably as a consequence of the dissipation processes that reduce the intensity of the Von Karman vortices.

4 Conclusions

Velocity 2D fields and in-flow pressure fluctuations were measured downstream a marine propeller in several axial and radial positions, for different advance ratios.

The performed experimental study permitted us to correlate the propeller flow field structures, like the blade wake and the tip vortex, with the pressure signal at a point. The results clarified that, within the slipstream contraction, the highest values of the pressure fluctuations correspond to a radial position $x/R = 0.9$, coinciding with the tip vortex passage. Thus this flow structure is the most important one in generating the hydrodynamic pressure field in the propeller flow.

Far downstream of the slipstream contraction the vortex breakdown occurs and the strong deformation of the hub vortex contributes to the pressure signal generation at the frequency of the shaft rate.

The standard deviation of the pressure signals shows the presence of two peaks, with different intensity, due to the blade wake, and the tip vortex passage. Furthermore, the increased values of the standard deviation in the downstream evolution point out that the vortex instability phenomena as also shown by the turbulence distribution.

The analysis conducted in the Fourier domain also evidenced the presence of narrow band pressure contributions due to the blade and shaft rotation rates as well as, in the high frequency range, to the shedding of vortices from the blades trailing edge.

Acknowledgments The authors are grateful to the CEIMM personnel and Mr. Giordano who supported the PIV measurements.

References

Cenedese A, Accardo L, Milone R (1985) Phase sampling techniques in the analysis of a propeller wake. First international conference on laser anemometry: advances and application, BHRA Fluid Engineering, Manchester

Di Felice F, Di Florio D, Felli M, Romano GP (2004) "Experimental investigation of the propeller wake at different loading condition by PIV" J Ship Res 48(2):168–190

Di Florio D, Di Felice F, Romano GP (2002) Windowing, reshaping and re-orientation of interrogation windows in PIV for the investigation of shear flows. Meas Sci Technol 48(2):168

Hoshino T, Oshima A (1987) Measurement of flow field around propeller by using a 3-component laser doppler velocimeter. Mits Technol Rev 24(1):46–53

Kobayashi S (1982) Propeller wake survey by laser doppler velocimeter. First international symposium on the application of laser anemometry to fluid mechanics, Lisbon

Min KS (1978) Numerical and experimental methods for prediction of field point velocities around propeller blades. Department of Ocean Engineering report 78–12, MIT

Saunders HE (1957) Hydrodynamic in ship design, SNAME

Stella A, Guj G, Di Felice F, Elefante M (2000a) Experimental investigation of propeller wake evolution by means of LDV and flow visualizations. J Ship Res 44(3):159–173

Stella A, Guj G, Di Felice F, Elefante M (2000b) Experimental investigation of propeller wake evolution by means of LDV and flow visualizations. Exp Fluids 28:1–10

Tachmindji AP, Dickerson MC (1957) The measurement of thrust fluctuation and free space oscillating for a propeller. Research and development report, report number 1107

Westerweel J (1997) Fundamentals of digital particle image velocimetry. Meas Sci Technol 8:1379–1392